Friction energy wear approach

Siegfried Fouvry

Friction energy wear approach

Siegfried Fouvry

Fretting Wear and Fretting Fatigue, Elsevier, pp.87-117, 2023,

Chapter : 3.2 Friction energy wear approach pp.87-117, 2023, Editors: Tomasz Liskiewicz, Daniele Dini, Elsevier ⟨10.1016/B978-0-12-824096-0.00006-8⟩

3.2 Friction energy wear approach

In general, fretting occurs between two tightly fitting surfaces that are subjected to a cyclic, relative motion of extremely small amplitude [1, 2]. For oxidizing metals, one of the immediate consequences of the process in normal atmospheric conditions is the production of oxide wear debris, hence the abusive term “fretting corrosion” was previously considered although the actual term of “fretting wear” is more consistent. Fretting movement is usually the result of external vibration, but in many cases, it is the consequence of one of the members of the contact being subjected to a cyclic stress (i.e. fatigue), which gives rise to another and usually more damaging aspect of “fretting fatigue” or “contact fatigue” [2]. Fatigue cracks are nucleated by the fretting contact stresses and propagate due to the bulk fatigue stress. The objective of this article is to focus on the fretting wear related to debris formation and ejection so the specific problematic of “fretting fatigue” will not be detailed presently. One illustration of fretting wear damage concerns the dovetail interface between the disk and the blades (Fig. 1). During the flight sequence (i.e. takeoff and landing) macro gross slip slidings are combined with aero-dynamical micro partial slidings which can generate combined fretting wear (i.e. wear volume induced by debris formation and debris ejection) but also fretting fatigue (i.e. crack nucleation and crack propagation).

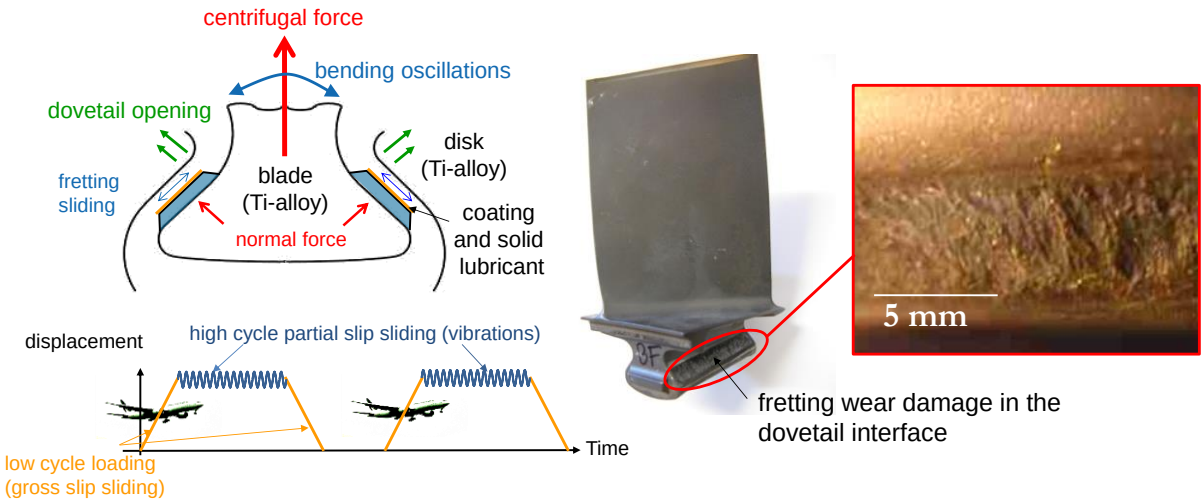

Fig. 1 : Illustration of fretting wear damage process in turbine engine dovetail interface [4].

Hence, there is a crucial interest to formalize how contact loadings like contact pressure, sliding amplitude but also contact size and ambient conditions can influence the fretting wear response.

3.2.1 Basics regarding friction energy wear approach

3.2.1.1 Fretting loop analysis and related friction energy parameters

Figure 2 illustrates the principle of a basic fretting wear test [3, 4]. This test configuration consists in applying a normal force P, a cyclic displacement δ_m (amplitude δ_m^*) using for instance a hydraulic or electromagnetic actuator. The latter alternated displacement results in a tangential force Q (amplitude Q*). The measured displacement δ_m is obtained from external extensometer (LVDT, laser sensor, …) where the loading forces (P & Q) are recorded from load cells.

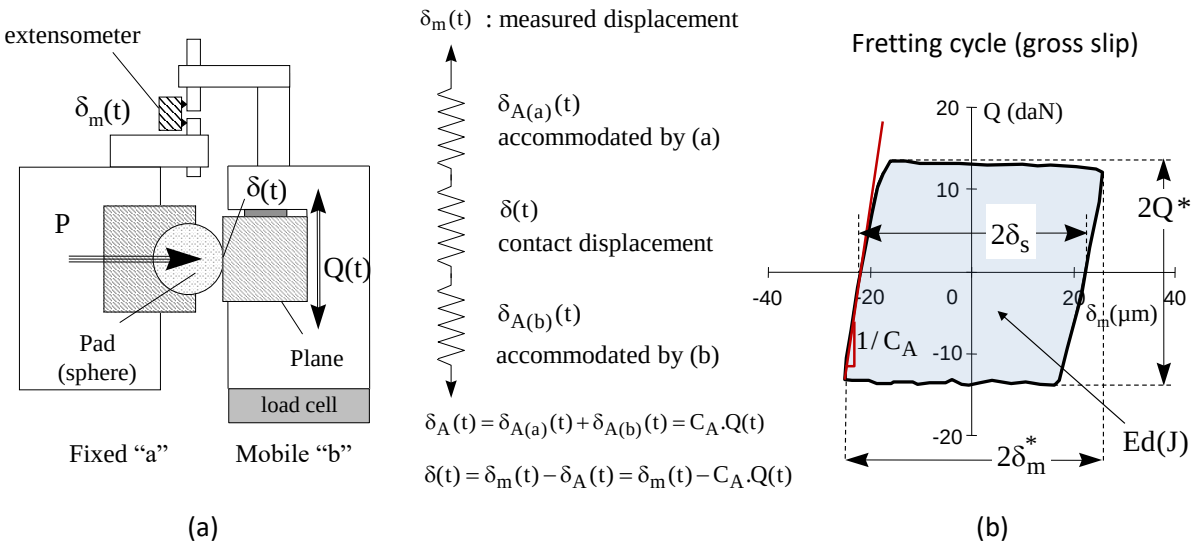

Fig. 2 : Schematic diagram of a basic fretting wear test and the related gross slip fretting cycle (After) [4].

It is interesting to note that the measured displacement amplitude δ_m^* is not equal to the contact displacement δ^* amplitude [**Erreur ! Source du renvoi introuvable.**]. Indeed, under small fretting oscillations, a significant part of the measured displacement is in fact accommodated by the test assembly deformation (δ_A). This latter depends on the applied tangential force and the compliance of the test assembly (C_A) which infers that (**Erreur ! Source du renvoi introuvable.**):

$$\boldsymbol{\delta_m^* = \delta^* + \delta_A = \delta^* + C_A \times Q^*} \quad (1)$$

The determination of C_A is long and fastidious. One alternative to estimate the real contact sliding amplitude (δ_s) consists in estimating the residual sliding amplitude when Q=0 on the ($\delta_m - Q$) fretting loop such that when Q=0, there is no more tangential deformation of the test apparatus (i.e. $\delta_s = \delta_m(Q=0) = \delta(Q=0)$).

Finally, by integrating the fretting loop, the friction energy $Ed\ (J)$ (i.e. friction work) inputted in the interface can be estimated. The accumulated friction energy $\Sigma Ed\ (J)$ (i.e. accumulated friction work) dissipated during the fretting test was indeed shown as a key parameter to formalize the wear volume extension [4, 5].

3.2.1.2 Archard versus friction energy wear concept: the influence of the coefficient of friction

Wear is a complex problem and many strategies were developed during the past decades to quantify this phenomenon in order to predict the wear volume extension.

Archard wear description

The usual strategy to quantify the wear rate in tribology consists in comparing the wear volume (V) extension a function of the Archard loading [6]. The Archard loading parameter is defined as the product of the normal force by the total sliding distance. For gross slip fretting sliding it is expressed by:

$$\mathbf{\Sigma W} = \sum_{\mathbf{i=1}}^{\mathbf{N}} \mathbf{4} \times \boldsymbol{\delta}_{\mathbf{S}}\,(\mathbf{i}) \times \mathbf{P}(\mathbf{i}) \qquad (2)$$

For constant loading conditions it is simplified to:

$$\mathbf{\Sigma W} = \mathbf{4} \times \boldsymbol{\delta}_{\mathbf{S}} \times \mathbf{P} \times \mathbf{N} \qquad (3)$$

Then, plotting the evolution of the wear volume V versus ΣW, linear correlations are approximated to determine the so-called wear coefficient K (mm3/ N.m) (or specific wear rate) so that:

$$\mathbf{V} = \mathbf{K} \times \mathbf{\Sigma W} \qquad (4)$$

One limitation of the Archard approach is that is does not consider the coefficient of friction in its formulation. Hence, under varying friction response a significant dispersion of the wear rate can be observed: the higher the coefficient of friction, the higher the wear rate (Fig. 3a) [7]. This can be interpreted using the K.L. Johnson diagram (Fig. 3b) [8] where the elastic (A), elastic shakedown (B) and plastic shakedown or ratcheting metal responses (C) are reported as a function of the friction coefficient and the applied contact pressure. After this approach, as long as the metal stabilizes under elastic response (A & B), the cumulated plastic deformation dissipation is zero or negligible. Alternatively, if it is doesn't stabilize (C), the plastic deformation is continuously increasing promoting high wear rates.

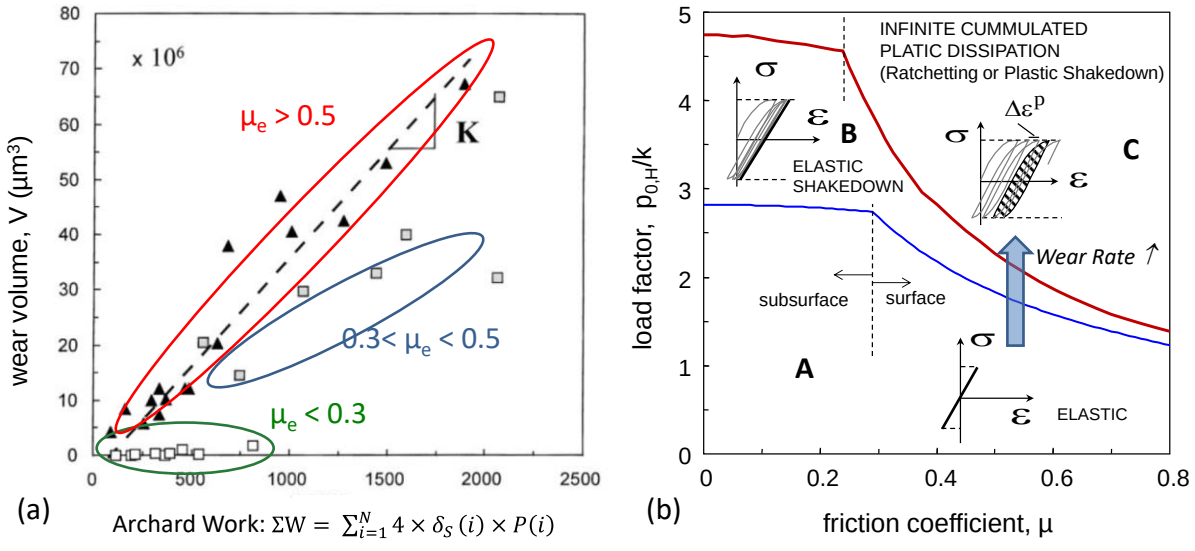

Fig. 3: (a) Analysis of the fretting wear extension of a sintered steel using Archard wear approach [7]; (b) K.L. Johnson displaying the various elastic and elastoplastic responses of metals as a function of the maximum Hertzian contact pressure and the friction coefficient (sphere-on-flat contact) [8].

3.2.1.3 Friction energy wear concept

An alternative strategy to quantify wear consists in considering the accumulated friction energy inputted in the fretted interface (i.e. accumulated friction work) (Fig. 4) [4, 5, 7].

$$\mathbf{\Sigma Ed} = \sum_{\mathbf{i=1}}^{\mathbf{N}} \mathbf{Ed(i)} \quad (5)$$

This approach is consistent with fretting analysis as it only requires summing the fretting loop area over the whole test duration. If the friction coefficient is constant, both Archard and friction energy approaches are equivalent such that:

$$\mathbf{\Sigma Ed} = \mu_{\mathbf{e}} \times \mathbf{\Sigma W} = \mathbf{4} \times \mu_{\mathbf{e}} \times \mathbf{\delta_S} \times \mathbf{P} \times \mathbf{N} \quad (6)$$

The wear volume extension is then quantified using an α energy wear coefficient:

$$\mathbf{V} = \boldsymbol{\alpha} \times \mathbf{\Sigma Ed} \quad (7)$$

Figure 11 confirms the stability of the friction energy wear approach to predict the fretting wear volume extension of TiC/alumina hard coating interface even for complex varying gross-slip sliding conditions [9].

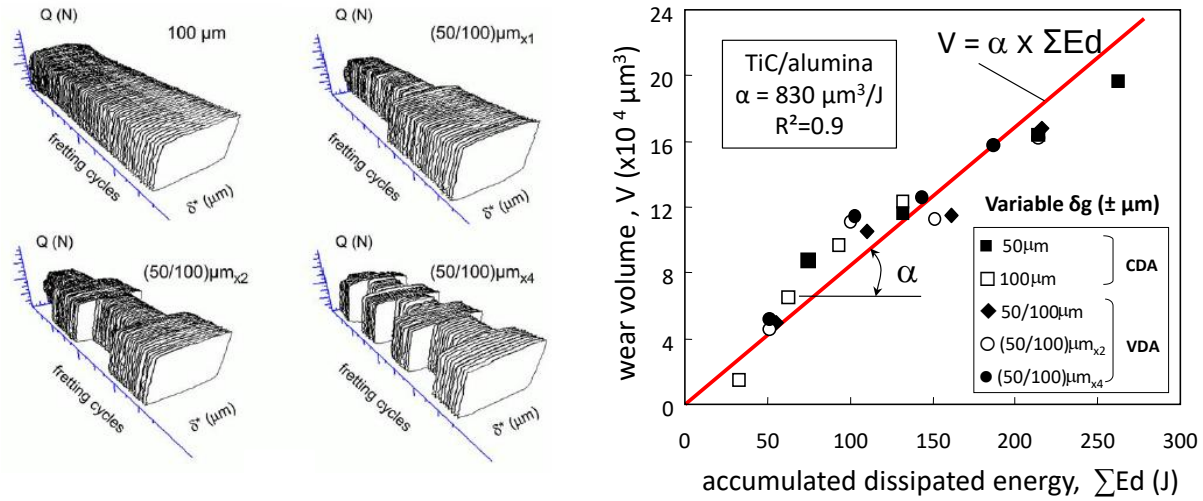

Fig. 4: Illustration how the friction energy wear approach is able to formalize the wear volume extension of a TiC/Alumina coating for constant (CDA) but also variable (VDA) gross slip displacement amplitudes (TiC/alumina) in a sphere-on-flat contact [9].

For metal interfaces, the friction energy wear approach also permits a better quantification of the wear volume extension. For instance, the former dispersive evolution observed for the sintered steel when using the Archard's parameter leads to quasi linear low dispersive tendency when considering the friction energy wear approach. This friction energy analysis also underlines the occurrence of a threshold friction $\mathrm{Ed_{th}}$ energy (along the X energy axis) which must be consumed by the fretted interface before generating the wear volume. This threshold evolution is typical for metallic interfaces such that before generating wear debris, plastic deformations of the metals (i.e. consuming a certain quantity of friction work), must be generated. This promotes a plastic

recrystallization process inducing the formation of the so-called Tribological Transformed Structure (TTS) which is very hard and very brittle [10-12]

Hence, the wear volume prediction can be corrected to consider the $\mathrm{Ed_{th}}$ energy offset so that [7, 10] (Fig. 5a):

$$\mathbf{V = \alpha \times (\Sigma Ed - Ed_{th})} \quad (8)$$

with $\mathrm{Ed_{th}}$ being the threshold incubation energy related to the transformation of the metal interface to TTS (Fig. 5b).

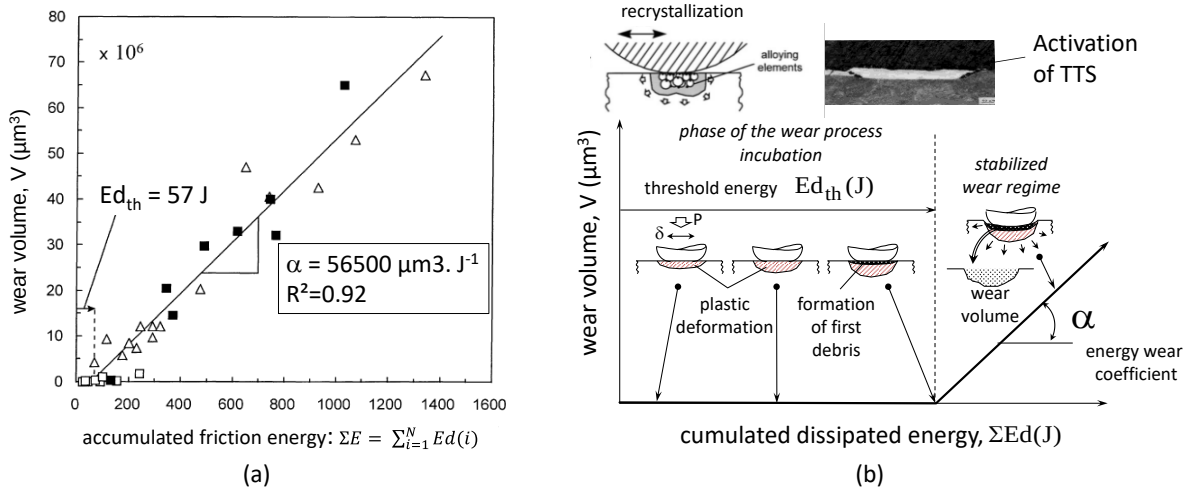

Fig. 5: (a) Evolution of the fretting wear volume of a sintered steel (Fig. 8a) versus the corresponding friction energy; (b) illustration of the fretting wear process related to metal interfaces (Incubation period related to the formation of TTS) [7].

To conclude, the friction energy appears as a pertinent approach to develop a more physical interpretation of the surface degradations. As illustrated in Fig. 6, many damage processes can be activated like cracking, plastic deformation, tribo-oxidation etc. However, some simulations investigating the energy balance involved in fretting damage processes suggested that in fact most of the friction energy is consumed by heating and third body flow ejection processes.

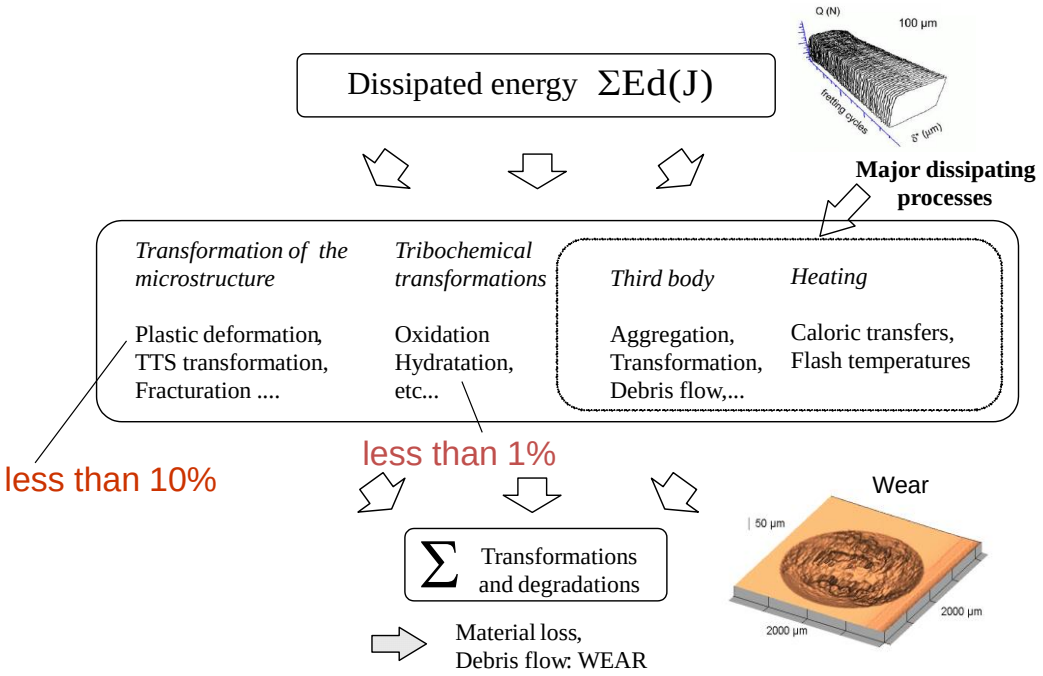

Fig. 6 : Illustration of the friction energy parameter as activator of surface damage processes [7].

3.2.1.4 Third body theory (TBT)

Archard and friction energy wear approaches are consistent as long as a similar wear process is activated. However, in many situations the wear volume extension cannot be described assuming a single wear coefficient. Indeed, like any other tribological phenomena, fretting wear is a very complex process which not only depends on the contacted materials but also on the contact system. A key aspect concerns the debris layer also called the third body or debris bed. Entrapped within the interface, it highly influences both friction and wear processes (Fig.7). Many investigations have been performed during the past decades to better quantify this aspect introducing the third body theory (TBT) [13-17]. After this theory, the wear rate evolution is not controlled by the friction work inputted in the interface but related to the balance between the debris formation flow ϕ_f generated from the degradation of the first body (bulk materials) and the debris ejection flow ϕ_e .

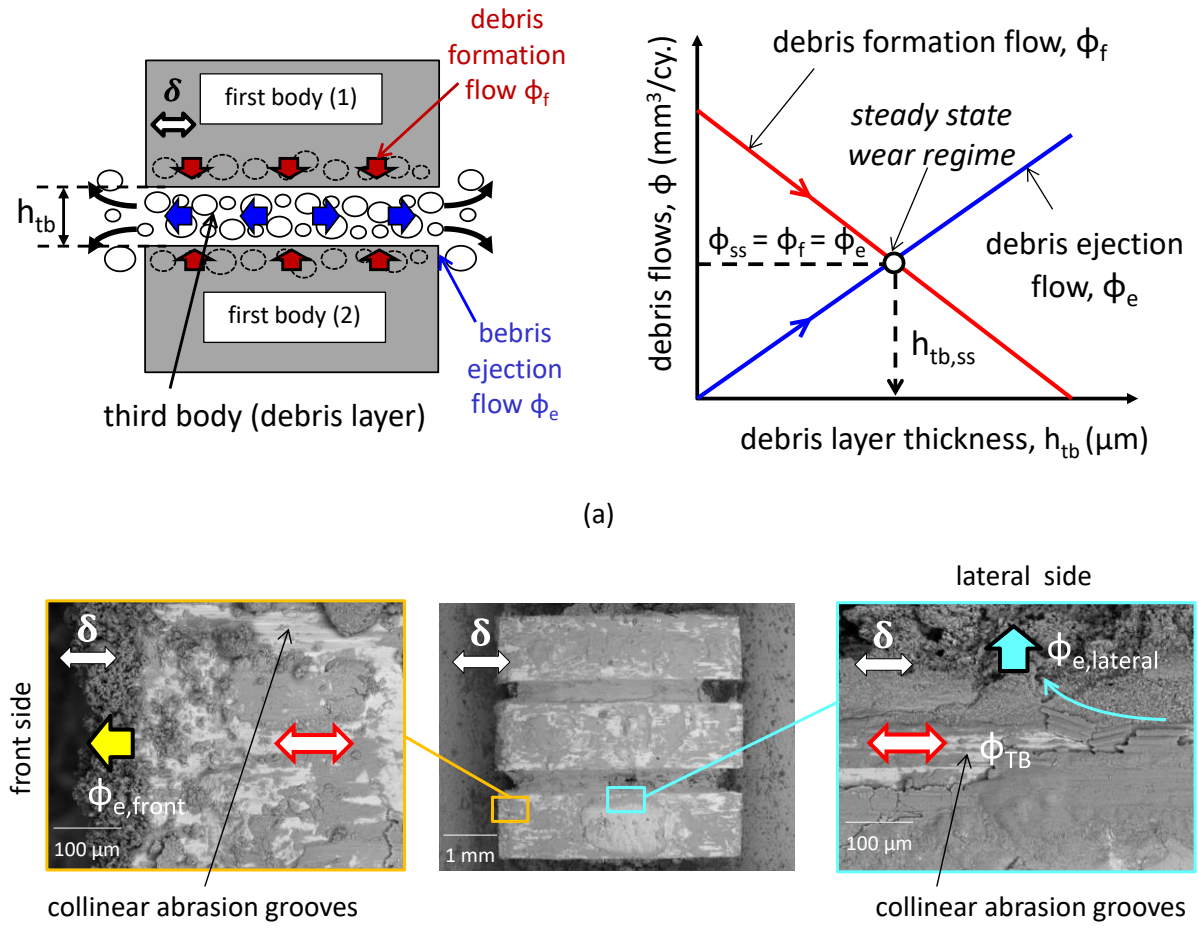

Fig. 7: (a) Schematic presentation of the third body theory and the debris flow concept as a function of the debris layer thickness [17]. (b) Illustration of the debris ejection flows observed at the contact opening of steel macro-textured flat-on-flat steel interface when the long edge is collinear to the sliding direction: most of the debris particles are ejected collinear to the sliding direction (primary flow) although a transverse ejection flow can be activated on the lateral sides (rotation of the debris path).

Figure 7a illustrates the principle of this theory where both debris formation and debris ejection flows are plotted versus the debris layer thickness: the thicker the debris layer (h_{tb}) the larger the debris ejection flow during each sliding sequence. However, the thicker the debris layer, the higher the friction energy consumed by the debris bed, the less damaged the first bodies, and finally the lower the debris formation flow. This theory suggests that the steady state wear regime corresponds to the situation when the debris formation flow equals the debris ejection flow:

$$\boldsymbol{\Phi_V = \Phi_f = \Phi_e} \qquad (9)$$

which also corresponds to a constant debris layer thickness ($h_{tb,ss}$).

Obviously, by modifying the contact condition another equilibrium point will be established inducing another steady state debris thickness.

3.2.1.5 Contact Oxygenation Concept (COC)

As detailed previously, the stability of the wear rate also depends on the stabilized wear mechanism. Fretting wear usually promotes either abrasive or adhesive wear phenomena. Abrasive wear implies a plowing process of the softer material by the harder asperities favoring the formation of oxide powder debris [18-19]. Abrasive wear favors debris ejection producing huge quantity of oxide particles. It generally leads to rather high wear rates.

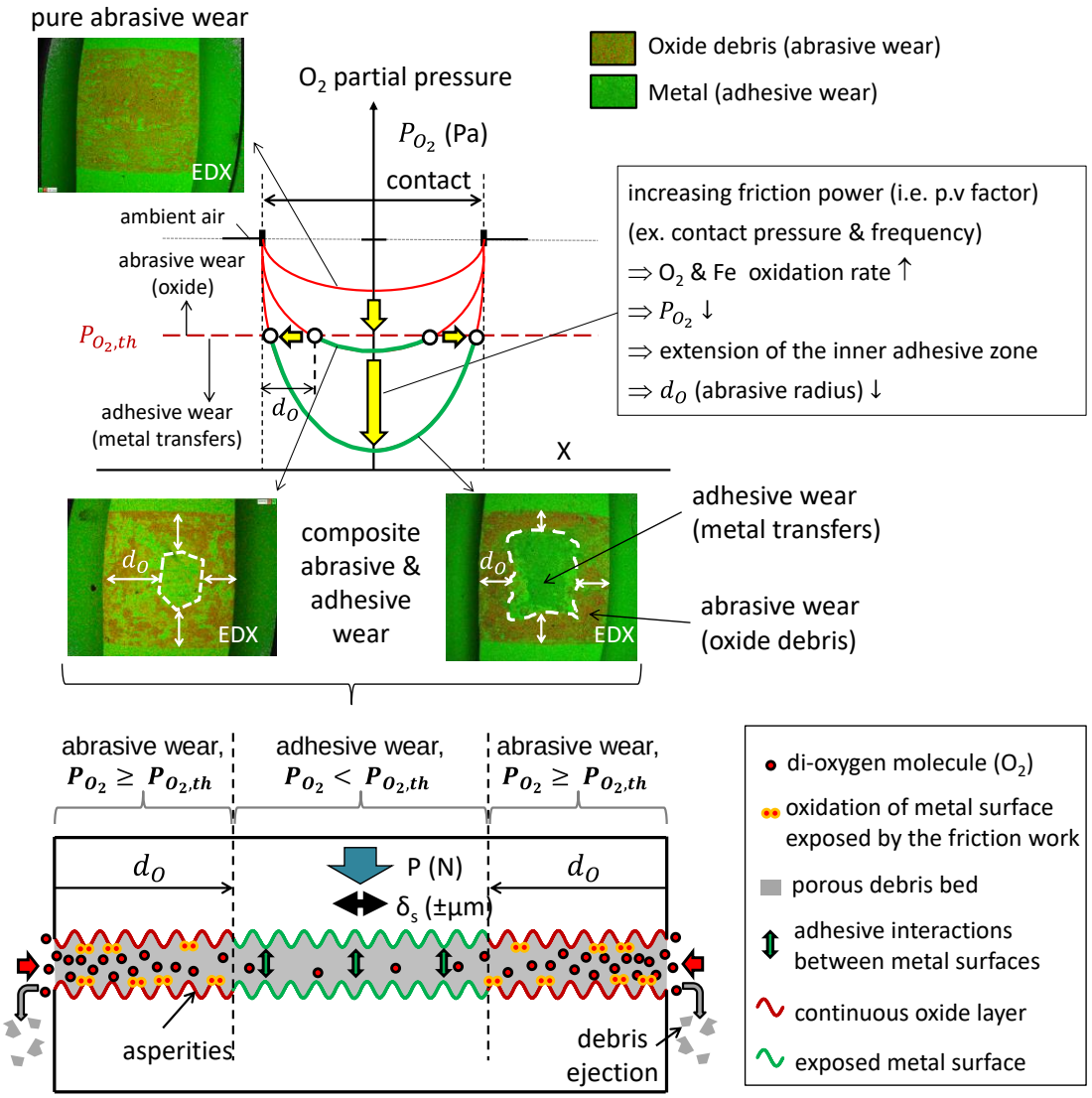

Fig. 8 : Illustration of the contact oxygenation concept (COC) formalizing the transition from pure abrasive to composite abrasive-adhesive fretting interface (experimental validation using crossed flat-on-flat interface) [20-22].

In contrast, adhesive wear phenomena inducing severe metal-metal transfers usually trigger rather low fretting wear rates since small sliding amplitudes limit the ejection of cohesive metal debris. However, catastrophic seizures inducing interface blocking are commonly observed. In many fretting interfaces both abrasive and adhesive wear phenomena are detected simultaneously. The partition between abrasive and adhesive process was recently formalized using the so-called contact oxygenation concept (COC) [20, 22] (Fig. 8), or equivalently air-distilling [23] or oxygen exclusion process [24]. Based on this concept, adhesive wear process is activated when the available di-oxygen partial pressure in the interface falls below a threshold value $P_{O2,th}$. The di-oxygen partial pressure is maximum at the contact borders (open air) but decreases toward the inner part of the contact due to the consumption of di-oxygen molecules reacting with the fresh metal to form oxide debris. The interface di-oxygen partial pressure profile can therefore be established as a balance between the di-oxygen diffusion rate from the external borders and the reaction rate with the metal surface exposed by the friction work. This concept was recently modeled using an Advection-Dispersion-Reaction model transposed by Baydoun et al. for fretting wear interfaces [22] (Fig. 9). By comparing the profile of the di-oxygen partial pressure in the interface, it is possible to predict the lateral extension of the abrasive wear domain (d_0) inner which the contact oxygenation is no more satisfied so that adhesive wear is occurring.

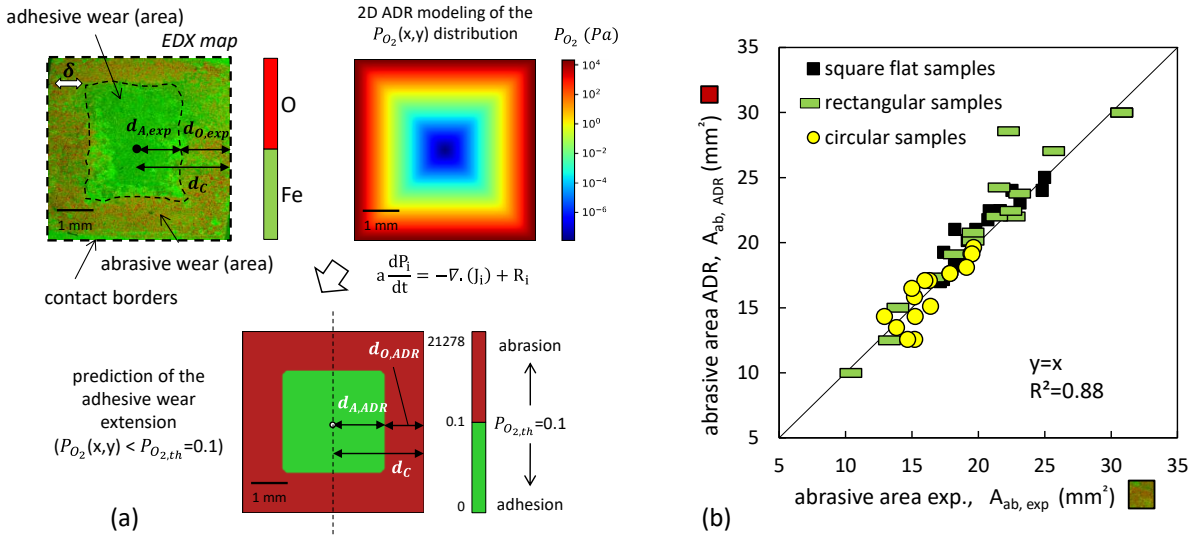

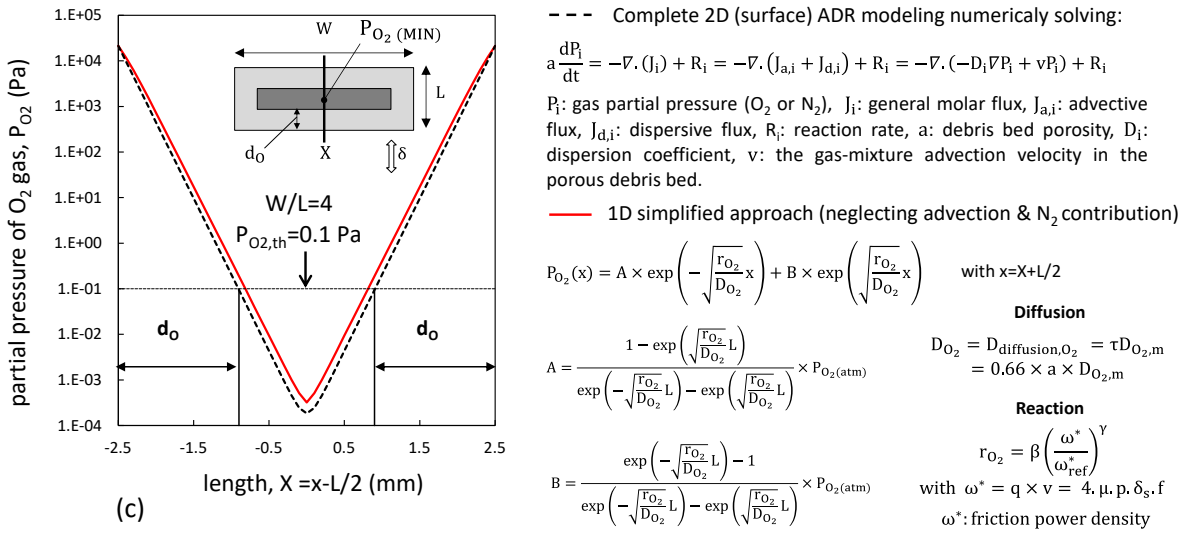

Fig. 9 : (a) EDX mapping of a 34NiCrMo16 flat-on-flat fretting contact (determination of the $\mathbf{d_{O,exp}}$ length scales by comparing the concentration of oxygen versus iron), modeling O_2 partial pressure within the fretted interface using the 2D complete ADR modeling (Advection-Dispersion-Reaction), prediction of the partition between abrasive and adhesive wear domains assuming $P_{O2,th}$ = 0.1 Pa [25]. (b) Comparison between experimental and predicted abrasive wear area in various square, rectangular and circular flat on flat contact configurations for a 34NiCrMo16/34NiCrMo16 interface [26]. (c) Comparison between 2D complete ADR modeling (1) and explicit formulation derived for 1D line contact neglecting advection contribution [26].

The comparison between experiments and simulations for a flat-on-flat steel interface confirms the stability of this approach. Note that adhesive wear in fretting was shown to be activated for an oxygen partial pressure not exceeding 0.1 Pa for a steel alloy tested under air-pressure controlled environments [25]. Based on this finding, it was assumed that $P_{O2,th}$ = 0.1 Pa being the threshold value below which steel interface was observed to activate pure adhesive wear process (Fig. 9a).

Note assuming an infinite transverse contact width and neglecting the advection contribution, a 1D explicit formulation of the local dioxygen partial pressure profile along the median axis of can be derived (Fig. 9b) [26]. The comparison with the complete 2D surface simulations confirms the stability of these simplified closed-form approximations .

3.2.2 Influence of contact loadings regarding friction energy wear rate (Dry & ambient temperature conditions)

3.2.2.1 Influence of the normal load

As the sliding amplitude, the wear rate coefficient would be assumed independent of the normal force such that this variable is already involved in the formulation the energy and Archard loading factors. The correlation of the wear extension versus normal force rather than the contact pressure is

justified by the Bowden and Tabor theory which suggests that the wear volume extension is indirectly proportional to the real contact area operating between asperities where plastic deformations of the contacting high spots (asperities) promote the formation of wear debris [27]. The real contact area (S) is directly proportional to the applied load (P) divided by the threshold contact pressure inducing plastic deformation (p_Y) which is itself approximately equal to $3\sigma_Y$, with Y being the yield stress in tension.

$$\mathbf{S} = \frac{\mathbf{P}}{\mathbf{p_y}} = \frac{\mathbf{P}}{\mathbf{3.\sigma_Y}} \quad (10)$$

The investigation of a flat-on-flat low alloyed steel interface (Fig. 19), allowing constant apparent contact area condition, confirmed that as long as the mean contact pressure remains lower than the threshold value (i.e. $p_{m,th} \approx 100$ MPa for the studied steel interface), the wear rate remains low and constant defining the so-called mild wear regime as predicted by the Archard and justified by Bowden and Tabor theories.

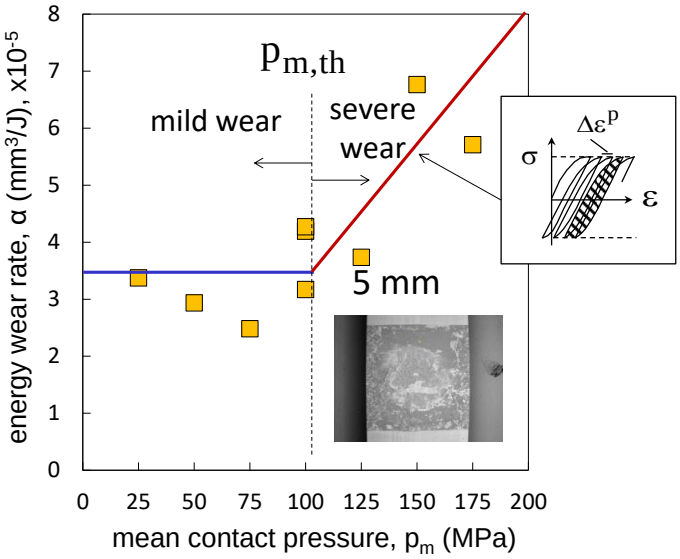

Fig. 10: Evolution of the wear rate of a flat-on-flat low-alloyed steel (34NiCrMo16) contact as a function of the mean contact pressure for gross slip fretting sliding [28].

However, above a threshold pressure, a sharp increase of the wear rate is observed defining the so-called severe wear regime. As illustrated previously, the transition from mild to severe fretting wear rate can be related to plastic shakedown or ratcheting (Fig. 3b).

3.2.2.2 Influence of the sliding frequency

Frequency is neither explicitly involved in the friction energy nor in the Archard wear parameter. However, this parameter was extensively investigated during the past decades [28-31]. This research

work underlines an increase of the wear rate when decreasing the sliding frequency (Fig. 11). This rise was related to the formation and disruption of oxide films. The longer the sliding period, the thicker the oxide layer removed after each sliding sequence and finally the higher the wear rate.

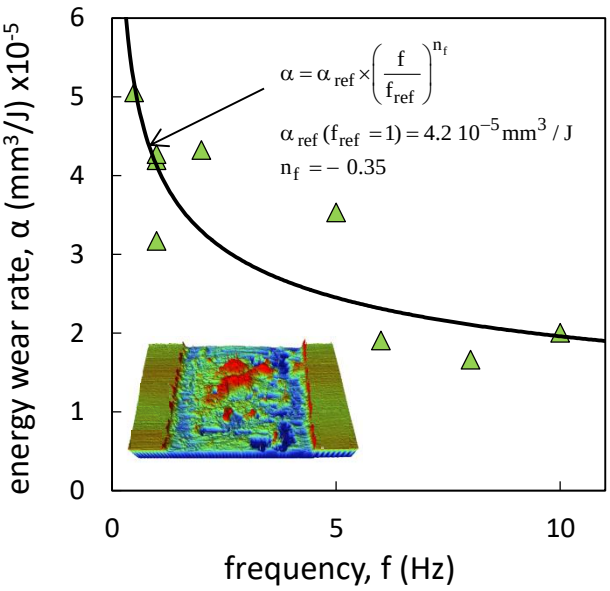

Fig. 11: Evolution of the energy wear rate as a function of the applied frequency (crossed flat 34NiCrMo16 steel) (28).

Various tribo-oxidation models suggest that the frequency dependency can be formalized using an Arrhenius formulation where the wear rate evolves as an inverse square root function of the frequency so that it be could expected a $1/f^{0.5}$ wear rate dependency [31].

Some fluctuation of the frequency exponent has been however observed (i.e. $\alpha \propto 1/f^{0.35}$) (Fig. 11) which can be explained assuming the "Contact Oxygenation Concept". Indeed, by increasing the sliding frequency and consequently the friction power dissipated in the interface, adhesive wear is extended and the global wear rate is consequently reduced because it does not only involve tribo-oxidation processes but also adhesive wear processes implying lower wear rates.

3.2.2.3 Influence of the contact size

Recent investigations underlines an asymptotic decreasing of the wear rate versus the contact size [17, 32-38] so that for Hertzian contact it infers that (Fig. 12a):

$$\boldsymbol{\alpha_L \approx \alpha_{ref} \times \frac{a_{H,ref}}{a_H}} \qquad (11)$$

This decreasing tendency was first explained by considering the third body theory (TBT) such that by increasing the contact size, the delay to eject the debris is longer, the debris ejection flow is reduced and consequently the wear rate is decreased. From this hypothesis it was concluded that the wear rate tends to zero for infinite contact size according that the debris can never be ejected from the interface [30, 38]. More recently contact oxygenation concept (COC) provided an additional

explanation particularly to explain the asymptotic evolution. Indeed, by increasing the contact size, the inner adhesive area is extended and because adhesive wear rate is smaller than the outer abrasive one, the global wear rate is reduced [17]. Hence the contact size effect was can therefore be addressed considering two L_{TBT} and L_{COC} contact length scale parameters [17]. Considering various rectangular contact sizes with L_C the collinear contact edge along the sliding direction and L_T the transverse edge it could be concluded that the TBT length scale may be related to L_C according that the debris flow is mainly driven by the alternated sliding process.

$$\mathbf{L_{TBT} = L_C} \quad (12)$$

Alternatively, assuming that contact oxygenation is isotropic, the COC length scale can be related to the minimum distance between the center of the contact and the ambient air which infers:

$$\mathbf{L_{COC} = \min(L_C, L_T)} \quad (13)$$

By combining plain and macro-textured interfaces allowing a wide range of L_C and L_T configurations, asymptotic decreasing of the wear rate were still observed whereas the global wear rate evolution versus the L_{TBT} and L_{COC} contact length scales was approximated using a power law function [17]:

$$\boldsymbol{\alpha_L = \alpha_{ref} \times \left[\frac{L_{COC}}{L_{COC,ref}}\right]^{n_{COC}} \times \left[\frac{L_{TBT}}{L_{TBT,ref}}\right]^{n_{TBT}}} \quad (14)$$

Rather nice correlations between experiments and the model (Fig. 12b) confirm the stability of the given L_{TBT} and L_{COC} contact size approach. Note that when L_{TBT} equal L_{COC} like for sphere/plane axi-symetrical interfaces, Eq. 14 becomes equivalent to Eq. 11, leading to a 1/L dependency.

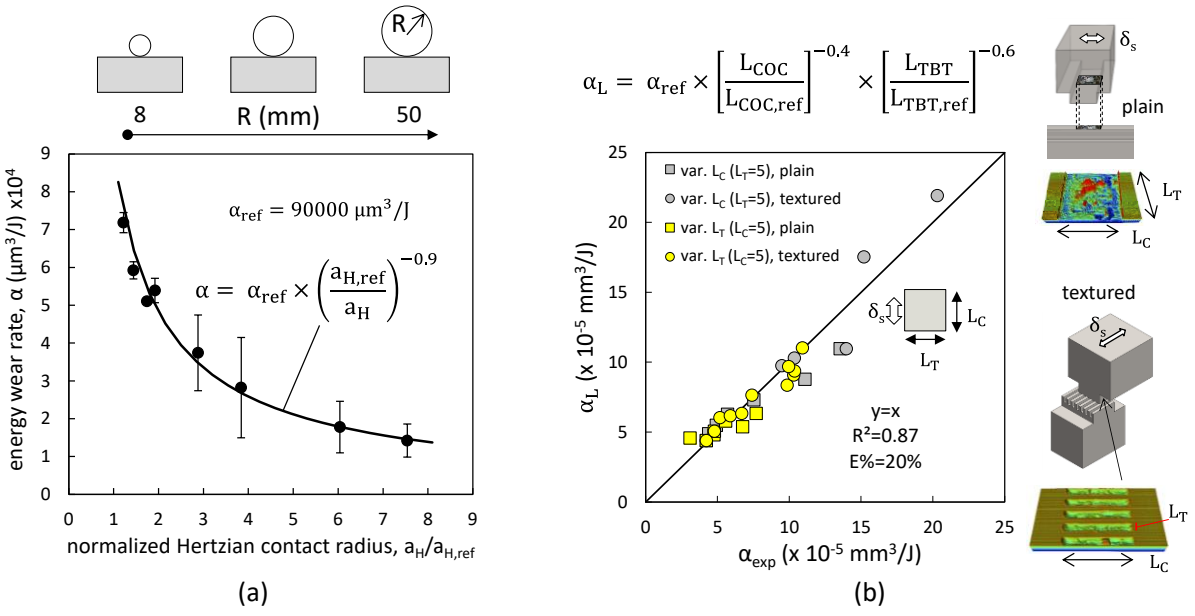

Fig. 12: (a) Evolution of the energy wear rate of 52100 sphere-on-flat contact versus the contact size (i.e. a_H Hertzian contact radius) [33], (b) comparison between experimental and power law prediction (α_L) of the wear rate fluctuation versus the contact size (34NiCrMo16 flat on flat steel interface,

N=20000 cycles, p=100 MPa, δ_s=±0.1 mm, f=1 Hz with $\alpha_{ref\ (L_C=L_T=5\ mm)}$= 4.23 10^{-5} mm^3/J, $n_{COC} = -0.4$ and $n_{TBT} = -0.6$ with $L_{COC,ref} = L_{TBT,ref} = L_{ref} = 5$ mm).

3.2.2.4 Influence of the sliding amplitude

The sliding amplitude variable is already involved in the computation of the accumulated friction energy and therefore the energy wear rate would be expected to be constant. Nonetheless, numerous fretting wear investigations highlighted an increase of the energy wear rate with the sliding amplitude particularly for adhesive wear materials [36-38]. This tendency can be explained considering the third body theory assuming that the larger the sliding amplitude, the easier the debris ejection flow and consequently the better the energy wear rate efficiency. Since both the contact size along the sliding direction "$L_C = L_{TBT}$" and the sliding amplitude "δ_s" display a reverse influence on the debris ejection it appears that the "L_{TBT}/δ_s" ratio appears as a pertinent variable to formalize the combined interaction of sliding amplitude and the TBT contact length scale [17] (Fig.).

$$\boldsymbol{\alpha_{L_{TBT},\delta_g} = \alpha_{ref} \times \left[\frac{L_{TBT}/\delta_s}{L_{TBT,ref}/\delta_{s,ref}}\right]^{n_{TBT}}} \quad (15)$$

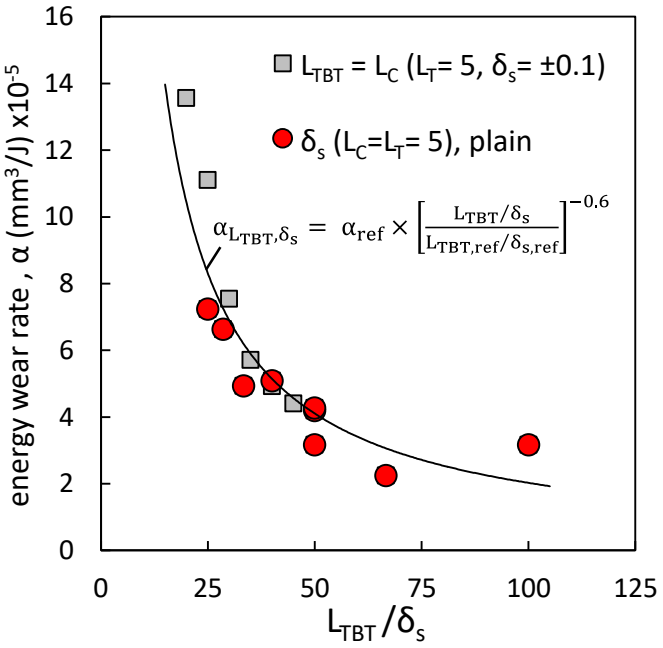

Fig. 13 : Evolution of the energy wear rate "α" versus the $\boldsymbol{L_{TBT}/\delta_s}$ ratio for plain and textured 34NiCrMo16 flat on flat steel interfaces (Fig. 5b) [17] (N=20000 cycles, p=100 MPa, f=1 Hz, (with $\boldsymbol{\alpha_{ref\ (L_C=L_T=5\ mm)}}$= 4.23 10^{-5} mm^3/J, $\boldsymbol{n_{TBT} = -0.6}$ with $\boldsymbol{L_{TBT,ref} = L_{ref} = 5\ mm}$, $\boldsymbol{\delta_s = \pm 0.1\ mm}$).

3.2.2.5 Extended wear coefficient approach: A power law formulation

These different investigations underline that the energy wear rate of a given interface cannot be considered constant but depends on many factors. The evolution of the energy wear rate under fretting wear conditions can be interpreted qualitatively considering the third body theory, the contact oxygenation concept or the plastic response of the interface. A key question concerns the quantitative formulation of such fluctuation. Various strategies can be applied; however it appears that a simple factorial power law function whose exponents related to each loading parameter can be derived from a restricted number of the experiments applying data optimization procedure [28, 17]:

$$\boldsymbol{\alpha^* = \alpha_{ref} \times \prod \left(\frac{X}{X_{ref}}\right)^{n_X}} \quad (16)$$

The contact loading parameter X can be substituted by L_{COC}, L_{TBT}, δ_s, p and f respectively which for the given flat-on-flat interface leading to [17]:

$$\boldsymbol{\alpha^* = \alpha_{ref} \times \left[\frac{L_{COC}}{L_{COC,ref}}\right]^{n_{COC}} \times \left[\frac{L_{TBT}/\delta_s}{L_{TBT,ref}/\delta_{s,ref}}\right]^{n_{TBT}} \times \left[\frac{p}{p_{ref}}\right]^{n_p} \times \left[\frac{f}{f_{ref}}\right]^{\eta_f}} \quad (17)$$

By defining this extended energy wear rate, the wear volume extension can be estimated:

$$\boldsymbol{V_{pred} = \alpha^* \times \sum Ed} \quad (18)$$

Figure 14 compares the experimental and the predicted wear volume derived from this extended friction energy wear rate approach. Rather good correlations with experiments confirm the stability of this approach which despite its simplicity, allows to take into account the effect of the contact size and the sliding amplitude through a synergic COC and TBT analysis, the effect of the contact pressure considering local plasticity at the asperity scale and the effect of frequency considering a tribo-oxidation contribution [17].

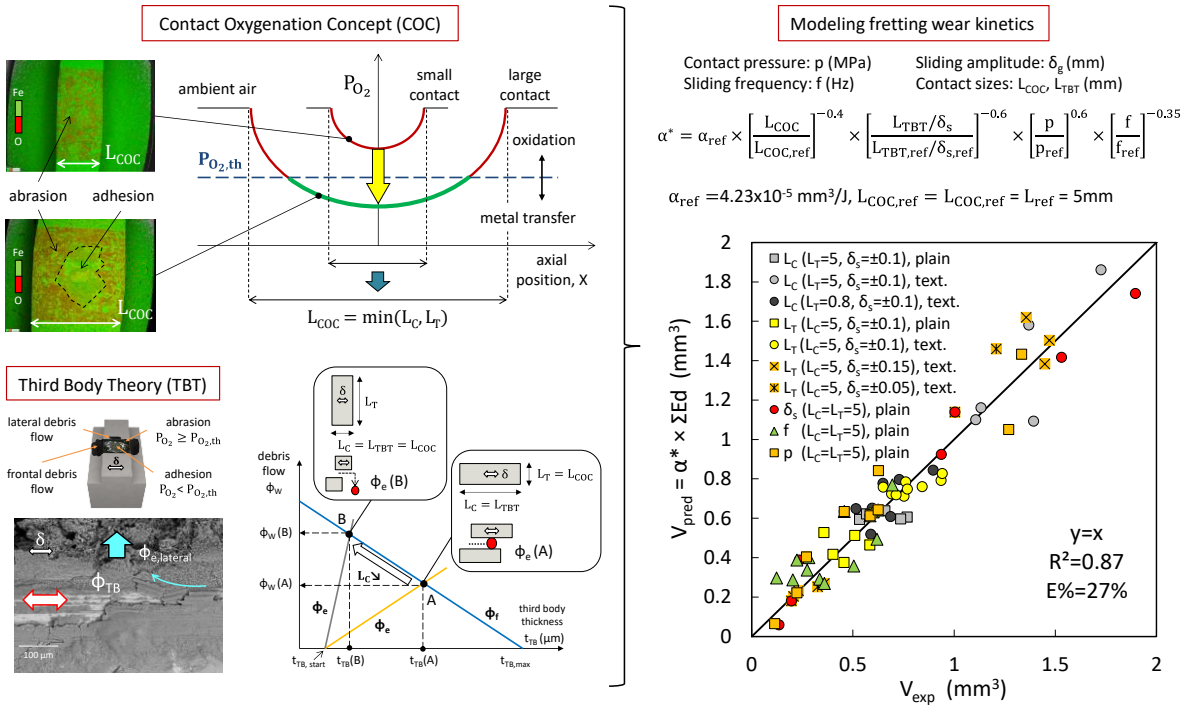

Fig. 14: Comparison between the experimental and the predicted wear volumes (Eq. 17, 18) of a 34NiCrMo16 flat on flat steel interface varying the contact size parameters L_C (mm), L_T (mm), the sliding amplitude δ_s (±mm), the frequency and the contact pressure [17] (except the mentioned conditions in the legend, the other loading parameters are kept constant at the reference conditions: N=20000 cycles, p_{ref}=100 MPa, f_{ref}= 1 Hz, $\delta_{s,ref}$= ±0.1 mm, α_{ref} =4.23x10^{-5} mm^3/J, $n_{COC} = -0.4$, $n_{TBT} = -0.6, n_p = 0.6$, $n_f = -0.35$, $L_{COC,ref} = L_{COC,ref} = L_{ref}$ = 5mm).

It must however be underlined that due to the complexity of tribology processes, it is not possible at this stage, to establish an a priori formulation of the "extended" energy wear coefficient without a specific "calibration" from a selected number of experiments. Note that this analysis describes the general case of a dry metal/metal interface at ambient temperature. Numerous investigations underlined a huge fluctuation of the energy wear rate depending on the temperature, lubricated or water ambient conditions justifying the developments of more advanced multiphysics modelings [38-39]. Some aspects of these influences are briefly illustrated in the following sections.

3.2.3 Influence of ambient conditions

3.2.3.1 Influence of temperature

Various fretting wear investigations underlined non-monotonic evolution of the wear rate with the temperature particularly for Inconel or stainless steel (i.e. cobalt based alloy) (Fig. 15). In the low and medium temperature range, the wear rate increases with the temperature due the synergic activation of the tribo-oxidation processes. However, above a threshold temperature, a tribo-sintering process of the debris layer is activated inducing the formation of a lubricious and above all

protective third body reducing the wear rate to nearly zero [30, 40, 41]. The process is reversible since when the temperature decreases below such a “glaze layer” threshold temperature (TGL), a linear high energy wear rate is observed again.

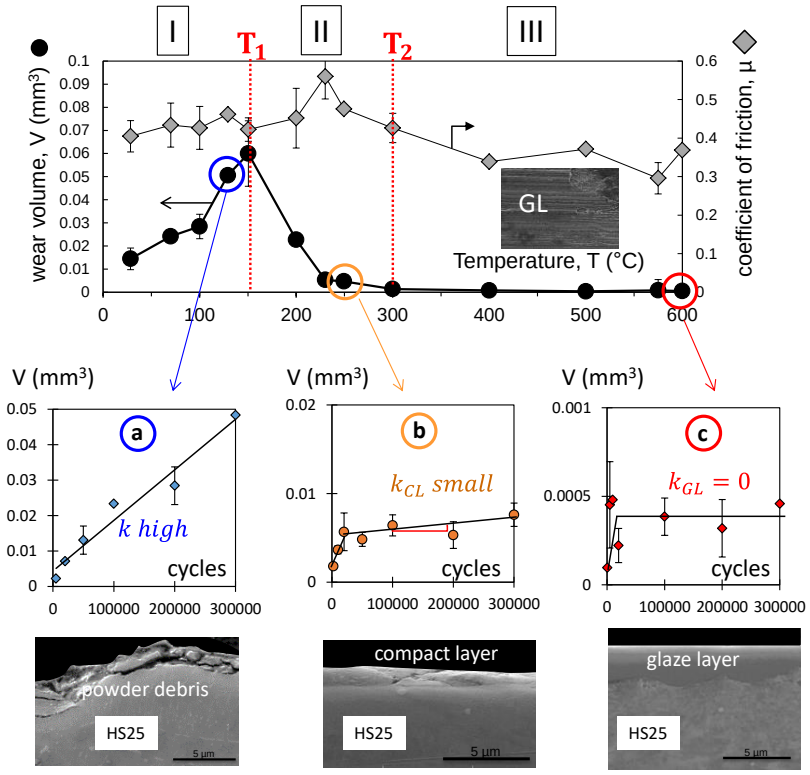

Fig. 15: Evolution of the fretting wear response of an HS25 Cobalt based alloy versus temperature. Activation of the lubricious and anti-wear glaze layer above T2 [41].

This peculiar behavior of the protective glaze layer was attributed to an over-adhesive property of the oxide debris under high temperatures. The friction energy still induces the wear debris formation, but the wear debris particles are so adhesive that they are immediately embedded and sintered in the compact and agglomerated third body layer. The debris cannot be ejected from the interface and finally the global wear rate converges to zero. The “glaze layer” temperature threshold (TGL) was shown to highly depend on the metal composition. The higher is the concentration of the highly diffusing element like cobalt or iron, the lower the TGL and therefore the better the high-temperature wear resistance. A complete wear rate formulation as a function of the applied temperature is detailed in [41]. The author demonstrated that using a restricted number of experiments and considering an Arrhenius – third body hypothesis it is possible to formalize such non monotonous evolution of the wear rate versus temperature.

3.2.3.2 Influence of lubricated (Grease) interface

Like temperature, lubricated interfaces under ambient conditions are mainly driven by the formation of specific tribofilms which in turn highly influence the wear rate evolution. Various authors [42-43] underlined that as long as the fretting contact is running under partial slip, the lubricant is ejected from the interface and the coefficient of friction remains very high as observed for dry contact (Fig. 16). However, because the friction energy under partial slip is very low, the wear volume is still negligible. Such high tangential force can induce high cyclic stresses which suggests that grease is not a pertinent palliative against fretting crack process. Note that even higher tangential force amplitudes as in dry contacts can be observed under partial slip condition such that the surrounding grease layer can prevent the access of di-oxygen molecules within the interface which tends to reduce severe adhesive metal/metal interaction. However, above the partial slip / gross slip transition, a reduction of the coefficient of friction can be observed. This reduction of the coefficient of friction is not related to a “hydrodynamic” process as the fretting sliding speed is still very small (less than few mm per second), but can be mainly explained by a “pumping” process which, by injecting some lubricant within the fretted interface, can promote the formation of lubricious tribofilms. Increasing the displacement and therefore the sliding amplitude, promotes a faster formation of the lubricious protective tribofilm so that above a threshold lubricated sliding amplitude, the wear volume extension converges nearly to zero. The measured wear volume is here equal to the initial transient wear volume generated before the formation of the tribofilm. Surface analysis underlined that this protective tribofilm is very adhesive and consists of a mixture or lubricant and oxide wear debris. Various investigations underlined that the lower the viscosity of the oil, the faster the lubrication and consequently the better the fretting wear response of the greased lubricated interface.

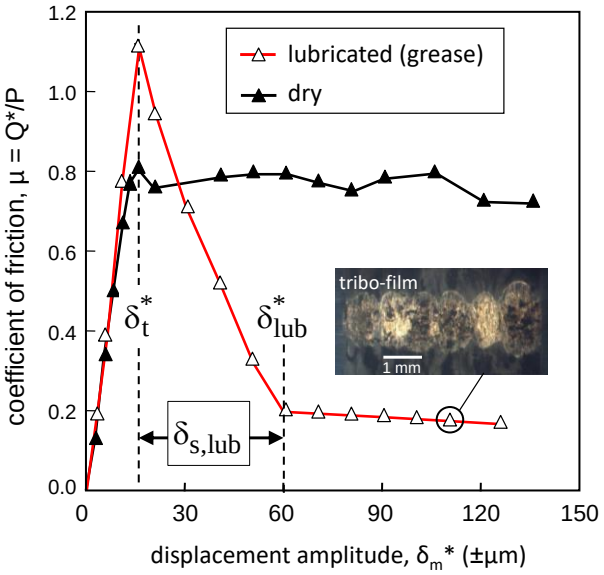

Fig. 16: Comparison of the stabilized friction coefficient (5000 cycles test duration) of a steel cylinder-on-flat smooth surface as a function of the applied measured displacement amplitude between dry and a grease-lubricated contact [44]).

3.2.4 Surface wear modeling using the friction energy density approach

3.2.4.1 Modeling the fretting worn profiles taking account the dynamical evolution of debris layer

Modeling the fretting wear profiles was extensively investigated during the past decades [45-49]. Different strategies like semi-analytical or boundary-element approaches could be adopted. However, for simple 2D contacts like the studied cylinder-on-flat interface, Finite Element Method (FEM) appears as a convenient approach as it is simple to implement surface wear simulations in common commercial codes. The first developments regarding fretting wear were undertaken by Mc Coll and co-author by considering a local Archard wear approach [45]. It was successively transposed to the energy wear approach considering a bilateral wear surface analysis of the contacted interfaces [46]. The surface wear modeling (Fig. 17a) consists in transposing the global wear volume approach at a local point of view where the total wear depth at a given x position is assumed proportional to the related accumulated friction energy density $\Sigma\varphi(x)$ through the corresponding energy wear coefficient:

$$\mathbf{h}(\mathbf{x}) = \boldsymbol{\alpha} \times \boldsymbol{\Sigma\varphi}(\mathbf{x}) \quad (19)$$

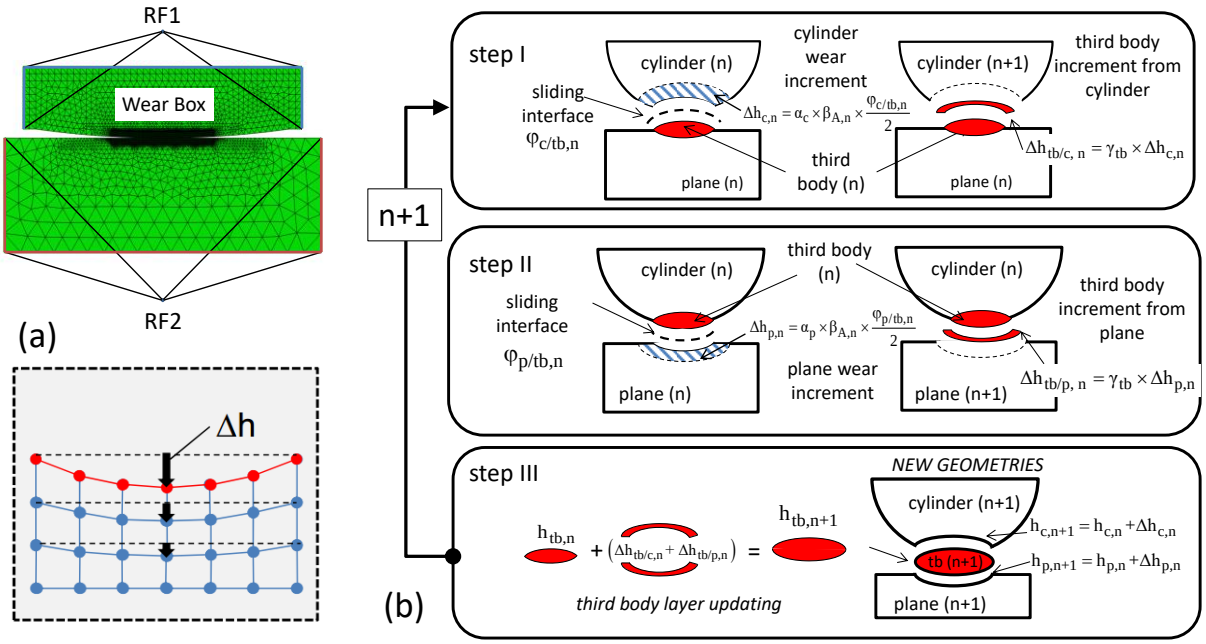

Fig. 17: Illustration of the surface wear modeling: (a) cylinder/plane FEM interface and node translation procedure to update the worn profile after the n^{th} iteration; (b) description of the three-step procedure to update the plane and the cylinder surfaces in addition to the third body layer [50].

These computations are long and fastidious, therefore to avoid the simulation of each experimental fretting cycle, an acceleration $\beta_{A,n}$ factor is considered. This acceleration factor expresses the number of real (experimental) fretting cycles approximated by each numerical fretting cycle. The $\beta_{A,n}$ variable must be chosen large enough to allow fast simulation but small enough to avoid numerical distortions [45, 46]. Transposed to the studied cylinder/plane interface, the numerical procedure consists in computing, the increment of wear generated on the plane and the cylinder surfaces at the iteration n, respectively:

$$\Delta h_{p,n}(x) = \alpha_p \times \beta_{A,n} \times \frac{\varphi_{p/c,n}(x)}{2}$$

and

$$\Delta \mathbf{h_{c,n}(x)} = \boldsymbol{\alpha_c} \times \boldsymbol{\beta_{A,n}} \times \frac{\boldsymbol{\varphi_{c/p,n}(x)}}{\mathbf{2}} \quad (20)$$

Where $\varphi_{p/c,n}(x)/2$ is the friction energy density reported on the two counterparts respectively, whereas α_p and α_c are the energy wear rates of the plane and cylinder respectively.

The contact geometry at the n numerical cycles is then updated by subtracting from the initial surface profile the computed worn thickness (h), so that a bilateral surface wear simulation could be achieved:

$$h_{p,n}(x) = h_{p,n-1}(x) - \Delta h_{p,n}(x)$$

$$\mathbf{h_{c,n}(x)} = \mathbf{h_{c,n-1}(x)} - \Delta \mathbf{h_{c,n}(x)} \quad (21)$$

Both plane and cylinder FEM geometries are then updated by applying a remeshing procedure. The final worn profiles are obtained when the number of simulated fretting cycles corresponds to a target (i.e. experimental) fretting cycle (N) so that:

$$\mathbf{N} = \sum_{\mathbf{n=1}}^{\mathbf{N_{num}}} \boldsymbol{\beta}_{\mathbf{A,n}} \quad (22)$$

This approach provides rather good surface wear simulations when the fretting contact is not influenced by the presence of a debris layer as observed in lubrication (like water). However, in dry contact when the debris particles display high cohesive properties, like for instance in Ti-6Al-4V interface, a thick third body layer is formed modifying, in consequence, the contact pressure and accordingly the wear profile evolution. Many researches intend to consider the presence of a debris layer in fretting wear simulation but considering a static description of this later [48, 49]. More recently, various authors [50, 51] proposed a dynamical approach where the third body layer is simulated as an additional FEM part entrapped between the interface evolving with the surface wear extension (Fig. 17b).

An originality of this approach lies in the fact that this third body layer extends laterally and in thickness as a function of the surface wear extension. Hence, after N numerical fretting cycle, a $\gamma_{\mathrm{tb,n}}(\mathrm{x})$ proportion of the worn thickness increment, so called third body conversion factor, is transposed to the third body layer. On the other hand, the $\mathrm{h}_{\mathrm{tb,n}}(\mathrm{x})$ thickness of the debris layer at the x position and at the n^{th} computation iteration evolves so that:

$$\mathbf{h_{tb,n}}(\mathbf{x}) = \mathbf{h_{tb,n-1}}(\mathbf{x}) + \boldsymbol{\gamma}_{\mathbf{tb,n}}(\mathbf{x}) \times (\Delta \mathbf{h_{p,n}} + \Delta \mathbf{h_{c,n}}) \quad (23)$$

Note that the complement of the third body transfer, (i.e. 1-$\gamma_{\mathrm{tb,n}}(\mathrm{x})$) corresponds to the proportion of the worn debris eliminated from the interface. The principle of this surface wear modeling taking into account the dynamical evolution of the third body layer is illustrated in Fig. 17b. Hence, by considering the local friction energy wear approach and simulating the presence and the evolution of the third body layer, it appears possible to better predict the fretting wear profile evolutions (Fig. 18a) as well as the maximum wear depth evolutions (Fig. 18b) which are key aspects to quantify the fretting wear durability of industrial assemblies.

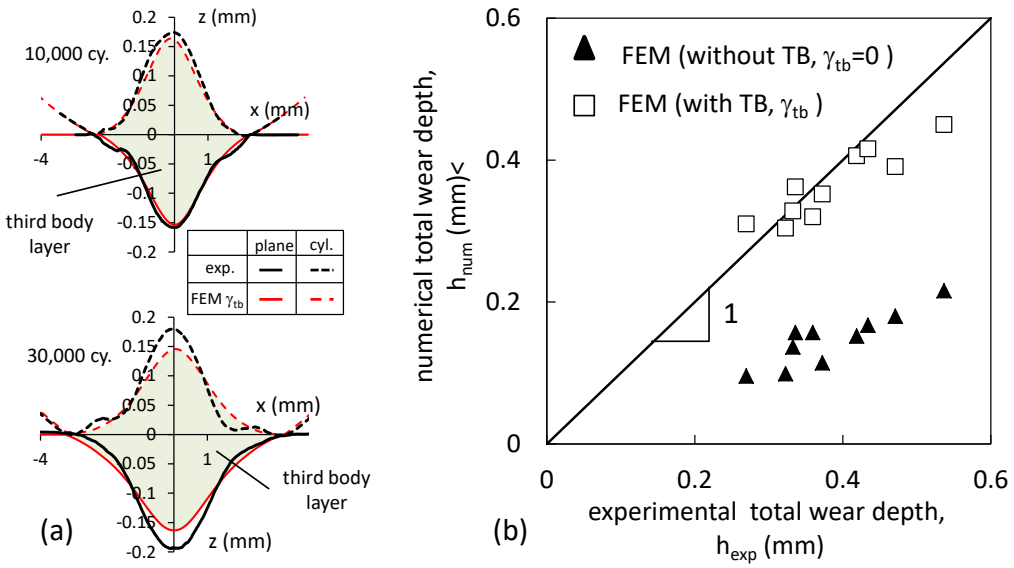

Fig. 18 : (a) Comparison between the experimental and the simulated worn profiles taking into account the presence of the third body through the third body conversion factor $\boldsymbol{\gamma_{tb,n}}$; (b) comparison between the experimental and the simulated maximum wear depth taking into account the presence of the debris layer [50].

3.2.4.2 Multiphysics fretting wear modeling including friction energy density, third body and contact oxygenation process.

This former fretting wear modeling taking account the dynamical evolution of debris layer is only validated when a single abrasive wear process operates within the interface inducing typical “U-shape” fretting scars. To simulate more complex abrasive-adhesive W-shape scar morphologies, a multi-physics approach combining mechanical friction energy and contact oxygenation concept need to be considered simultaneously [39] (Fig. 19).

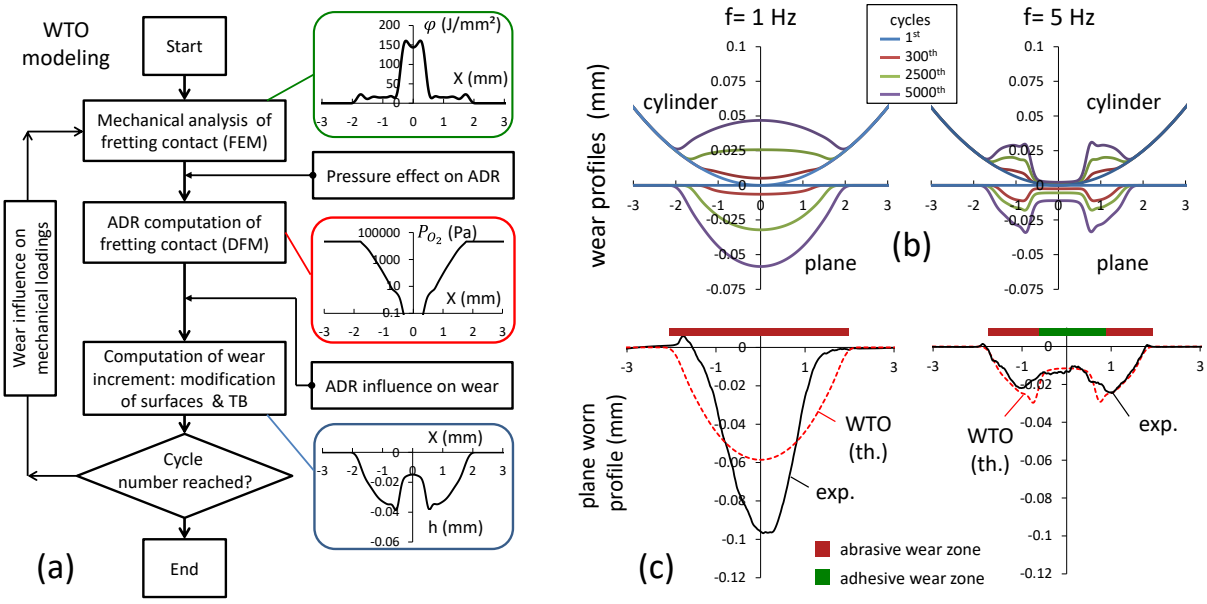

Fig. 19: (a) Global algorithm of the WTO multiphysics wear modeling combining friction energy (i.e. mechanical), third body simulation and ADR simulation of the contact oxygenation process [39], (b) Multi-physics simulation (WTO) of plane and cylinder worn profiles and debris layer thickness profiles as a function of the applied sliding frequency, (c) Comparison between WTO and the experimental wear profiles as a function of the applied sliding frequency (b & c: Ti-6AL-4V cylinder-on-flat interface, R= 80 mm, $F_{n,L}$ =1066 N/mm, δ_s= ±75 µm, N=5000 cycles) [39].

This so-called WTO multiphysics wear modeling (i.e. Wear modeling including Third body and contact Oxygenation) allows capturing the evolution of the fretting scar when varying the sliding conditions. It can for instance predict the evolution of the fretting scar from "U" shape morphology when the abrasive wear process is operating over the whole fretted interface (i.e. $P_{O2}>P_{O2,th}$) for low sliding frequency until the typical "W" fretting scar structure when adhesive wear phenomenon is operating within the inner part of the contact under high sliding frequency conditions (Fig. 19b). Despite its simplicity and limitations, rather correlations with experiments were observed underlying the potential interest of such tribological approach to predict complex fretting wear processes and seizure phenomena as well.

4.2.4.3 Predicting the coating durability using the friction energy density parameter

Many technological developments have been developed during the past decades to improve the wear resistance applying soft, hard and solid lubricant coatings. These surface treatments reduce the coefficient of friction and limit seizure phenomena [9, 52-56]. Their performances are usually established by comparing the wear volume extension although in practice the coating durability needs to be related to the critical loading cycles (Nc) when the sliding interface reaches the substrate

interface. For solid lubricant coatings, Nc can be easily detected by measuring the discontinuous increase of the coefficient of friction (Fig. 20a). When the coating doesn't lead to significant fluctuation of the coefficient of friction, Nc can be estimated by performing interrupted tests and measuring the maximum wear depth. The coating durability Nc can be expressed as a function of the applied displacement amplitude for a given normal load as detailed by Langlade et al. [54] (Fig. 20b). It can be also formalized as a function of the maximum friction energy density (or Archard density parameter) inputted in the fretted interface (Fig. 20c). Investigating thin coating layers (i.e. less than few micron thicknesses), the worn surface extension can be then neglected so that the initial maximum friction energy density appears as a reliable parameter to establish the fretting wear durability of coatings. Using this approach, contact pressure and sliding amplitude can be combined through a single energy loading variable. A power law formulation can be defined so that the coating endurance can be related to a given friction energy capacity (χ) [9, 55-57] characterizing the fretting performance of a given surface treatment (i.e. coating).

$$\mathbf{Nc} = \frac{\chi}{\varphi_{max}} \tag{24}$$

with φ_{max} being the maximum friction energy density inputted in the contact during a fretting cycle given by:

$$\boldsymbol{\varphi_{max}} = \mathbf{4} \times \boldsymbol{\delta_s} \times \mu_e \times \mathbf{p_{max}} \tag{25}$$

where p_{max} is the maximum pressure value in the contact.

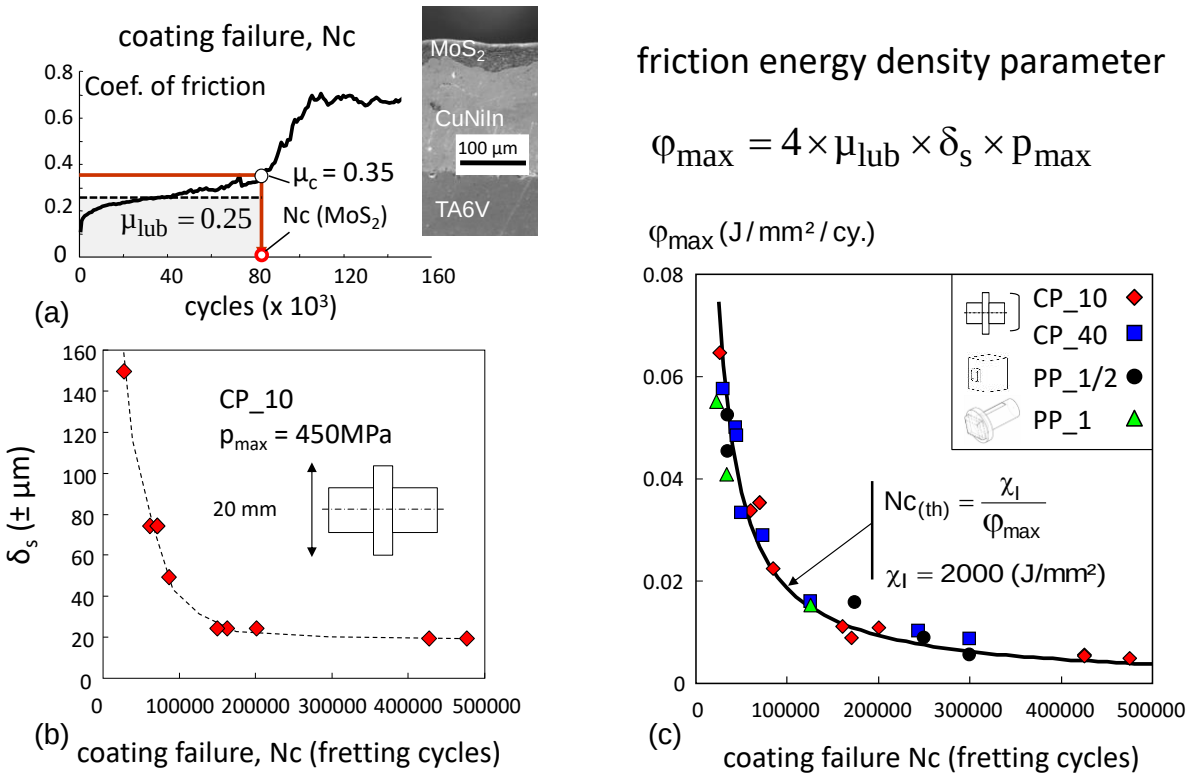

Fig. 20: Quantification of the coating durability under fretting wear (analysis of an MoS2 solid lubricant) [56]: (a) coating failure Nc when the substrate is reached (friction discontinuity), (b) evolution as a function of δ_s; (c) quantification of Nc as a function of the maximum local friction energy density for various contact geometries (CP: cylinder/plane, PP: punch/plane), sliding amplitude (δ_s) and maximum contact pressure (p_{max}).

For hard coating layers (i.e. TiC PVD coating, [9]), the friction energy capacity could be related to the energy wear coefficient (α) assuming a linear extension of the maximum wear depth versus the maximum accumulated friction energy density so that (Fig. 21):

$$\boldsymbol{\chi} = \frac{\mathbf{t_n}}{\boldsymbol{\alpha}} \qquad (26)$$

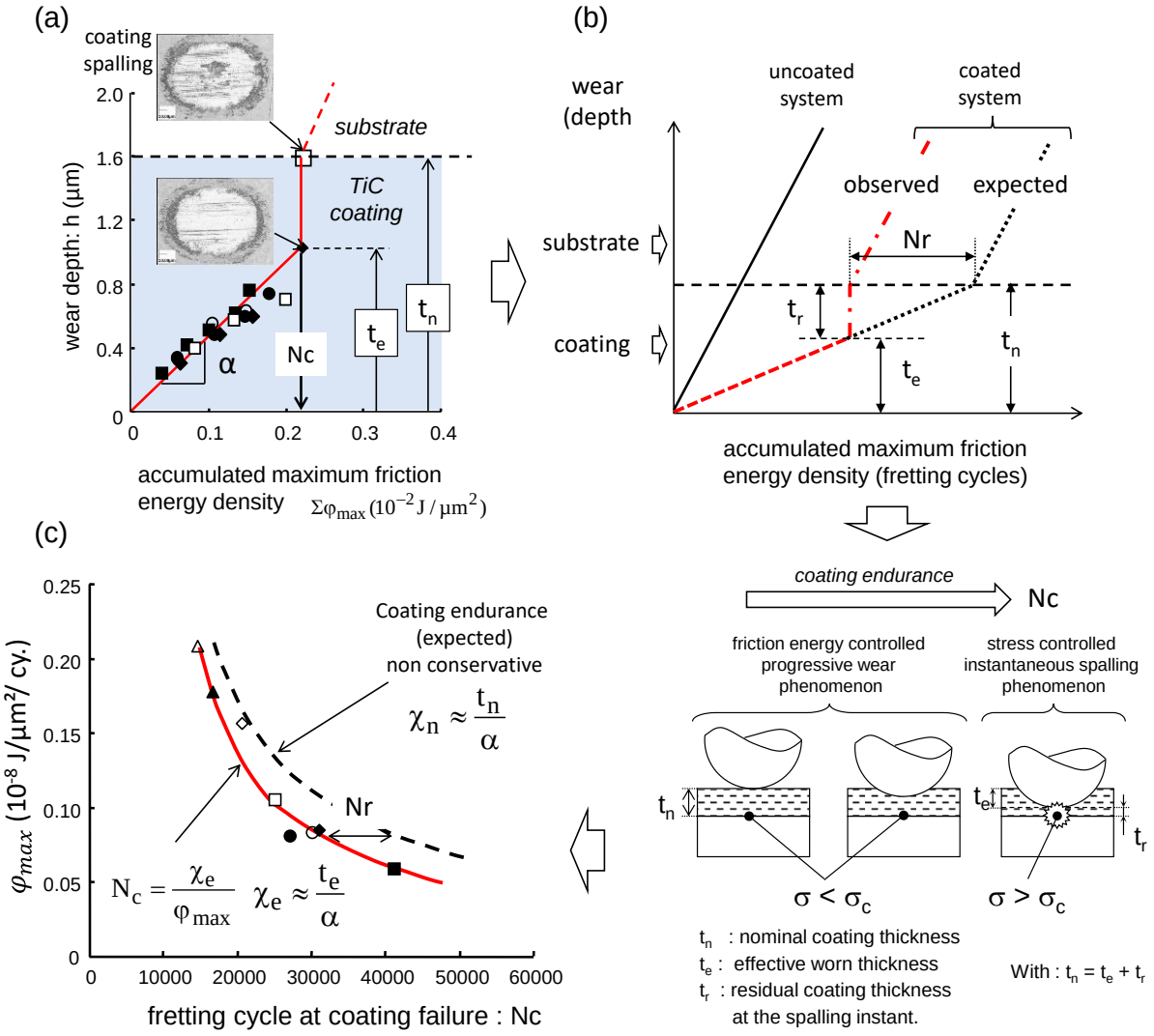

Fig. 21: Application of the friction energy density approach to formalize the fretting wear durability of a thin TiC hard coating [9]: (a) evolution of the maximum wear depth as a function of the accumulated friction energy density; (b) coating failure occurring at h = t_e due to brutal decohesion phenomenon so that an effective coating thickness (t_e) smaller than the nominal one (t_n) must be considered to rationalize the coating durability; (c) formalization of the coating durability Nc as a function of the maximum friction energy density inputted in the interface $\boldsymbol{\varphi_{max}}$ through the effective friction energy capacity of the studied TiC coating ($\boldsymbol{\chi_e}$).

However, in many situations, brutal spalling phenomenon inducing a coating failure before the fretted interface reaches the substrate can be observed. This significantly reduces the expected fretting wear endurance. This aspect can be formalized by considering the effective coating thickness (t_e) related to the worn thickness before the coating layer is definitively removed from the interface due to a cracking cohesion process so that [9] (Fig. 21):

$$\mathbf{Nc} = \frac{\chi_e}{\varphi_{max}} \quad (27)$$

with

$$\chi_e = \frac{t_e}{\alpha} = \frac{t_n - t_r}{\alpha} \quad (28)$$

with t_r being the residual coating thickness just before failure. Hence, using this basic approach it is possible to formalize the fretting wear endurance of hard coatings like TiC.

3.2.5 Conclusion

This chapter illustrates some aspects regarding the quantification of the fretting wear degradation using the friction energy approach. Because friction energy takes into account the friction coefficient, it appears more reliable than the usual Archard work theory in predicting the fretting wear volume extension at least under fluctuating friction coefficient conditions. However, many investigations underline that the energy wear coefficient (α) is not constant but depends on the wear mechanics involved in the fretted interface which itself depends on the loading conditions. To interpret such fluctuations both Third Body Theory (TBT) and Contact Oxygenation Concept (COC) must be considered. Third Body Theory (TBT) suggests that the wear kinetics is a function of the balance between the debris formation and the debris ejection flows. The Contact Oxygenation Concept (COC) allows formalizing the transition from abrasive to adhesive wear response when the dioxygen partial pressure within the debris layer becomes lower than a threshold value (i.e. $P_{O2}(x,y) < P_{O2,th}$). Hence, the fresh metal exposed by the friction work cannot be oxidized so metal transfers are activated. Using TBT and COC, it is possible to interpret and rationalize the effect of contact pressure, sliding frequency, sliding amplitude but also contact size effects regarding the fluctuation of the energy wear rate parameter. Multiphysics models combining friction energy density, third body conversion parameter but also ADR approach were recently developed to formalize, at the local scale, the surface damage evolution observed in the fretting scars. Using this multiphysics strategy, pure abrasive “U-shape” but also abrasive-adhesive “W-shape” fretting scar morphologies can be approximated. Besides, by better predicting the wear depth extension it is also possible to better predict the durability of fretting wear palliatives like solid lubricants but also hard coatings.

List of symbols

Latin letters

d_O : distance from the interface boundaries to the frontiers of the adhesion zone (abrasive wear extension) [µm]

d_A : width of the inner part of the contact enduring adhesive wear [µm]

f : frequency [Hz]

h : total wear depth (i.e. sum of the two counterfaces) [µm]

$h(x)$: total wear depth profile (i.e. sum of the two counterfaces) at the x position [µm]

$h_{c,n}(x)$: cylinder worn profile at the n^{th} fretting cycle

h_{max} : total maximum wear depth (i.e. sum of the two counterfaces) [µm]

$h_{p,n}(x)$: plane worn profile at the n^{th} fretting cycle [µm]

$h_{tb,n}(x)$: thickness of the third body layer at the n^{th} fretting cycle [µm]

K : Archard wear coefficient [mm^3/(N.m)]

N : applied fretting cycles

N_C : fretting cycle related to the coating failure

p : contact pressure [MPa]

P : normal force [N]

p_m : mean contact pressure [MPa]

p_{max} : maximum contact pressure [MPa]

Q : tangential force [N]

Q^* : tangential force amplitude [N]

P_{0_2} : di-oxygen partial pressure within the interface [Pa]

S : apparent contact area [mm²]

T : temperature [°C]

t : time [s]

t_n : nominal coating thickness [µm]

t_e : effective coating thickness [µm]

V : Wear volume [mm^3 or μm^3]

Greek letters

α : total (global contact) energy wear coefficient [mm^3/J]

α_c : energy wear coefficient of cylinder surface [mm^3/J]

α_p : energy wear coefficient of plane surface [mm^3/J]

$\beta_{A,n}$: number of real fretting cycles simulated during the n^{th} numerical fretting cycle (acceleration factor)

$\gamma_{tb,n}$: third body conversion factor (proportion of the worn thickness transferred to the third body layer at the n^{th} fretting cycle)

δ : effective contact displacement [µm]

δ_A : displacement accommodated by the test apparatus [µm]

δ_m : measured displacement [µm]

δ_m^* : measured displacement amplitude [µm]

$\delta_{m,t}^*$: measured displacement amplitude at the gross slip transition [µm]

δ_s : effective sliding amplitude [µm]

$\delta_{s,lub}$: effective sliding amplitude inducing lubrication in grease interface [µm]

δ_t^* : effective contact displacement at the sliding transition [µm]

$\Delta h_{p,n}$: increment of the wear depth generated on the plane surface during the n^{th} cycle [µm]

$\Delta h_{c,n}$: increment of the wear depth generated on the cylinder surface during the n^{th} cycle [µm]

μ : nominal friction coefficient

μ_e : energy friction coefficient

ΣW : accumulated Archard work [N.m]

$\Sigma\varphi(x)$: accumulated friction energy density dissipated at the x position [J/mm²]

ΣEd : accumulated friction energy (i.e. friction work) [J]

σ_Y : plastic yield stress [MPa]

ϕ : debris flow

$\varphi(x)$: friction energy density dissipated at the x position during a fretting cycle [J/mm²]

φ_{max} : maximum friction energy density dissipated in the interface during a fretting cycle [J/mm²]

χ : friction energy capacity [mm²/J]

References

[1] D. Hoeppner, Mechanisms of fretting fatigue and their impact on test methods development, ASTM STP 1159 (1992) 23–32.

[2] R.B. Waterhouse, Fretting wear, Wear 100 (1–3) (1984) 107-118.

[3] Z.R. Zhou, S. Fayeulle, L. Vincent, Cracking Behaviour of various aluminium alloys during fretting wear, Wear 155 (1992) 317-330.

[4] S. Fouvry, P. Kapsa, V. Vincent, Quantification of fretting damage. Wear 200 (1-2) (1996) 186-205.

[5] H. Mohrbacker, B. Blanpain, J.P. Celis, J.R. Roos, L. Stals, M. Van Stappen, Oxidational wear of TiN coatings on tool steel and nitride tool steel in unlubricated fretting, Wear 188 (1995) 130-137.

[6] J.F. Archard, J. F., Contact and rubbing of flat surfaces. Journal of Applied Physics 24(8) (1953) 981.

[7] S. Fouvry, Ph. Kapsa, An Energy Description of Hard Coatings Wear Mechanisms, Surface & Coating Technology, 138 (2001) 141-148.

[8] K.L. Johnson, Contact Mechanics, Cambridge University Press, 1985, Cambridge.

[9] T. Liskiewicz, S. Fouvry, Development of a friction energy capacity approach to predict the surface coating endurance under complex oscillating sliding conditions, Tribology International 38 (1) (2005) 69-79.

[10] E. Sauger, S. Fouvry, L. Ponsonnet, P. Kapsa, J. M. Martin et al., Tribologically transformed structure in fretting, Wear 245(1) (2000) 39-52.

[11] V. Nurmi, J. Hintikka, J. Juoksukangas, M. Honkanen, M. Vippola, A. Lehtovaara et al. The formation and characterization of fretting-induced degradation layers using quenched and tempered steel, Trib. Int. (2019) 258–67.

[12] D. Tumbajoy-Spinel, S. Descartes, J.-M.l Bergheau , V. Lacaille, G. Guillonneau , J. Michler , G. Kermouche, Assessment of mechanical property gradients after impact-based surface treatment: application to pure α-iron, Materials Science & Engineering A 667 (2016) 189–198.

[13] M. Godet, Third-bodies in tribology, Wear 136 (1990) 29-45.

[14] N. Fillot, I. Iordanoff, Y. Berthier, Modeling, Third body flows with a discrete element method—a tool for understanding wear with adhesive particles, Trib. Int. 40 (2007) 973–981.

[15] S. Descartes, Y. Berthier, Rheology and flows of solid third bodies: background and application to an $MoS_{1.6}$ coating, Wear 252 (2002) 546–556.

[16] A.M. Kirk, P.H. Shipway, W. Sun, C.J. Bennett, The effect of frequency on both the debris and the development of the tribologically transformed structure during fretting wear of a high strength steel, Wear 426 (2019) 694–703.

[17] Soha Baydoun, Siegfried Fouvry, Sylvie Descartes, Modeling contact size effect on fretting wear: a combined contact oxygenation - third body approach, Wear 488–489 (2022) 204168

[18] K. Holmberg, A. Matthews, Properties, Mechanisms, Techniques and Applications in Surface Engineering, Elsevier Science, 2009, ISBN: 9780444527509 (p. 576).

[19] G.W. Stachowiak, Wear, Materials, Mechanics and Practice, Tribology in Practice Series, WILEY, ISBN 0470016280, 458 pages.

[20] S. Fouvry, P. Arnaud, A. Mignot, P. Neubauer, Contact size, frequency and cyclic normal force effects on ti-6al-4v fretting wear processes: An approach combining friction power and contact oxygenation. Trib. Int. 113 (2017) 460-473

[21] S. Baydoun, S. Fouvry, An experimental investigation of adhesive wear extension in fretting interface: Application of the contact oxygenation concept, Trib. Int. 147 (2020) 106266.

[22] S. Baydoun, P. Arnaud, S. Fouvry, Modeling adhesive wear extension in fretting interfaces: An advection-dispersion-reaction contact oxygenation approach, Trib. Int. 151 (2020) 106490.

[23] C. Mary, S. Fouvry, J.M. Martin, B. Bonnet, Pressure and temperature effects on Fretting Wear damage of a Cu–Ni–In plasma coating versus Ti17 titanium alloy contact, Wear 272 (1, 3) (2011) 18-37.

[24] A.R. Warmuth, S.R. Pearson, P.H. Shipway, W. Sun, The effect of contact geometry on fretting wear rates and mechanisms for a high strength steel, Wear 301(1–2) (2013) 491–500.

[25] A. Iwabuchi, T. Kayaba, K. Kato, Effect of atmospheric pressure on friction and wear of 0.45% C steel in fretting. Wear 91 (1983) 289–305.

[26] S. Baydoun, P. Arnaud, S. Fouvry, Explicit formulations of adhesive wear extension in fretting interfaces applying the contact oxygenation concept, Wear 488-489 (2022) 204147

[27] F.P. Bowden, D. Tabor, The Friction and Lubrication of Solids, Oxford University Press, 1950

[28] S. Baydoun, S. Fouvry, S. Descartes, P. Arnaud, Fretting wear rate evolution of a flat-on-flat low alloyed steel contact: A weighted friction energy formulation, Wear 426 (2019) 676–693.

[29] R.B. Waterhouse, Fretting, Treatise on Materials Science and Technology, D. Scott, Ed., Academic Press, 1978, 259–286.

[30] X. Jin, P.H. Shipway, W. Sun, The role of temperature and frequency on fretting wear of a like-on-like stainless steel contact, Tribo. Lett. 65, article 77 (2017).

[31] A. Dreano, S. Fouvry, G. Guillonneau, A tribo-oxidation abrasive wear model to quantify the wear rate of a cobalt based alloy subjected to fretting in low-to-medium temperature conditions, Trib. Int. 125 (2018) 128–140.

[32] S. Fouvry, C. Paulin, S. Deyber, Impact of contact size and complex gross–partial slip conditions on Ti–6Al–4V/Ti–6Al–4V fretting wear Tribology International 42 (3) (2009) ,461-474.

[33] Merhej, S. Fouvry, Contact size effect on fretting wear behaviour: application to an AISI 52100/AISI 52100 interface, Lubr. Sci. 24 (2012) 273–290.

[34] S. Fouvry, R. Merhej, Introduction of a power law formulation to quantify the contact size effects on friction and wear responses of dry oscillating sliding contacts: Application to a chromium steel interface, Wear 301 (2013) 34–46.

[35] T. Zhu, P.H. Shipway, W. Sun, The dependence of wear rate on wear scar size in fretting; the role of debris (third body) expulsion from the contact, Wear. 440–441 (2019) 203081.

[36] S. Fouvry, P. Duo, Ph. Perruchaut, A quantitative approach of Ti-6Al-4V fretting damage: Friction, Wear and crack nucleation, Wear 257(9-10) (2004) 916-929.

[37] T. Zhu, P.H. Shipway, Contact size and debris ejection in fretting: The inappropriate use of Archard-type analysis of wear data and the development of alternative wear equations for commonly employed non-conforming specimen pair geometries, Wear 474–475 (2021) 203710.

[38] P.H. Shipway, A.M. Kirk, C.J. Bennett, T. Zhu, Understanding and modeling wear rates and mechanisms in fretting via the concept of rate-determining processes - Contact oxygenation, debris formation and debris ejection, Wear 486–487 (2021) 20406.

[39] P. Arnaud, S. Baydoun, S. Fouvry, Modeling adhesive and abrasive wear phenomena in fretting interfaces: A multiphysics approach coupling friction energy, third body and contact oxygenation concepts, Trib. Int. 161 (2021) 107077.

[40] F.H. Stott, G.C. Wood, The influence of oxides on the friction and wear of alloys, Trib. Int. 11 (1978) 211–218.

[41] A. Dreano , S. Fouvry, G. Guillonneau, Understanding and formalization of the fretting-wear behavior of a cobalt-based alloy at high temperature, Wear 452(2020) 203297.

[42] M. Shima, H. Suetake, I.R. McColl, R.B. Waterhouse, M. Takeuchi, On the behaviour of an oil lubricated fretting contact, Wear 210 (1997) 304–310.

[43] Z.R. Zhou, L. Vincent, Lubrification in fretting a review, Wear 225(9) (1999) 962–968.

[44] S. Fouvry, V. Fridrici, C. Langlade, Ph. Kapsa, L. Vincent, Palliatives in Fretting : A dynamical approach, Tribology International 39 (2006) 1005–1015.

[45] I.R. McColl, J. Ding, S.B. Leen, Finite element simulation and experimental validation of fretting wear, Wear 256, (2004) 1114–1127.

[46] C. Mary, S. Fouvry, Numerical prediction of fretting contact durability using energy wear approach: Optimisation of finite-element model, Wear 263(1-6) (2007) 444-450.

[47] L. Gallego, B. Fulleringer, S. Deyber, D. Nelias, Multiscale computation of fretting wear at the blade/disk interface, Tribol. Int. 43(4) (2010) 708–718.

[48] S. Basseville, G. Cailletaud, An evolution of the competition between wear and crack initiation in fretting conditions for Ti-6Al-4V alloy, Wear 328 (2015) 443–455.

[49] T. Yue, A. l. Wahab, Finite element analysis of fretting wear under variable coefficient of friction and different contact regimes, Tribology International 107 (2017) 274-282.

[50] P. Arnaud, S. Fouvry, A dynamical FEA fretting wear modeling taking into account the evolution of debris layer, Wear 412–413 (2018) 92-108.

[51] V. Done, D. Kesavan, M. Krishna R, T. Chaise, D. Nelias, Semi analytical fretting wear simulation including wear debris, Tribol. Int. 109 (2017) 1–9.

[52] Z. B. Cai, Z. Yang Li, M. G. Yin, M. H. Zhu, Z. R. Zhou, A review of fretting study on nuclear power equipment, Tribology International 144 (2020) 106095.

[53] Daniel Toboła, Tomasz Liskiewicz, Liuquan Yang, Thawhid Khan, Łukasz Boroń, Effect of mechanical and thermochemical tool steel substrate pre-treatment on diamond-like carbon (DLC) coating durability, Surface & Coatings Technology 422 (2021) 127483.

[54] C. Langlade , B. Vannes , M. Taillandier , M. Pierantoni, Fretting behavior of low-friction coatings: contribution to industrial selection, Tribology International 34 (2001) 49–56.

[55] V. Fridrici, S. Fouvry, Ph. Kapsa, Ph. Perruchaut, Impact of contact size and geometry on the lifetime of a solid lubricant, Wear 255 (2003) 875-882.

[56] Fouvry, C. Paulin, An effective friction energy density approach to predict solid lubricant friction endurance: Application to fretting wear, Wear 319 (2014) 211–226.

[57] T. Liskiewicz, S. Fouvry, B. Wendler, Development of a Wöhler-like approach to quantify the hard coatings durability under oscillating sliding conditions, Wear 259 (1-6) (2005) 835-841.